

Modeling geometry of planar hydraulic fractures using the Planar 3D ILSA approach

A.V. Valov¹, A.N. Baykin^{1,2}, E.V. Dontsov³

¹ Lavrentyev Institute of Hydrodynamics SB RAS

² Novosibirsk State University, Russia

³ W.D. Von Gonten Laboratories, Houston, USA

Novosibirsk,
1 July, 2019

Outline

- Mathematical model
- Tip asymptotic solution
- Implicit level set algorithm
- Model verification
- Contact algorithm
- Coupling with proppant transport

Planar3D ILSA Model (Peirce, Dontsov, 2017)

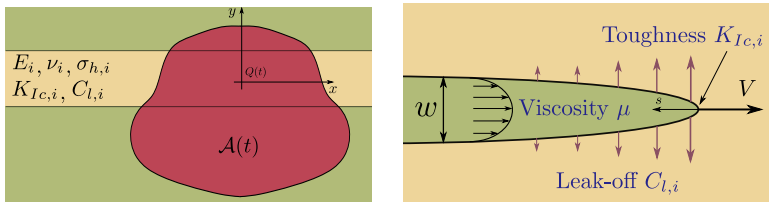


Figure 1 : Scheme of planar hydraulic fracture in layered medium.

**Elasticity
equation**

$$p(x, y, t) = \sigma_h(y) - \int_{\mathcal{A}(t)} w(x', y', t) G(x, y, x', y') dx' dy',$$

$$G_{\text{homogeneous}}(x, y, x', y') = \frac{E'}{8\pi [(x' - x)^2 + (y' - y)^2]^{3/2}},$$

**Lubrication
equation**

$$\frac{\partial w}{\partial t} = \frac{1}{\mu'} \nabla \cdot (w^3 \nabla p) - \frac{C'}{\sqrt{t-t_0(x, y)}} + Q(t) \delta(x, y),$$

**Boundary
conditions**

$$\lim_{s \rightarrow 0} \frac{w}{s^{1/2}} = \frac{K'}{E'}, \quad \lim_{s \rightarrow 0} w^3 \frac{\partial p}{\partial s} = 0.$$

Tip asymptotic solution

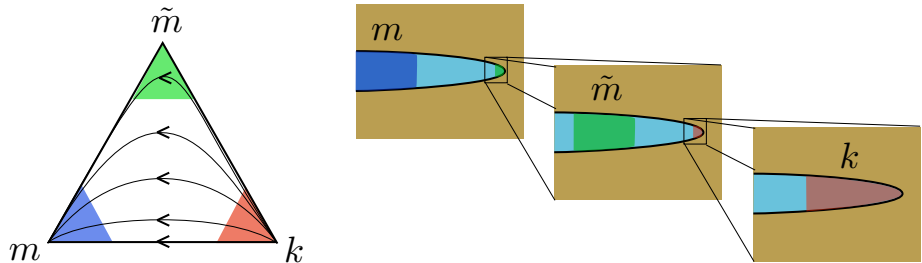


Figure 2 : Parametric triangle corresponding to the all asymptotic regimes: k is toughness dominated, \tilde{m} is leak-off dominated, m is viscosity dominated.

$$w_k = \frac{K'}{E'} s^{1/2}, \quad w_{\tilde{m}} = \beta_{\tilde{m}} \left(\frac{4\mu'^2 V C'^2}{E'^2} \right)^{1/8} s^{5/8}, \quad w_m = \beta_m \left(\frac{\mu' V}{E'} \right)^{1/3} s^{2/3}.$$

Discrete equations

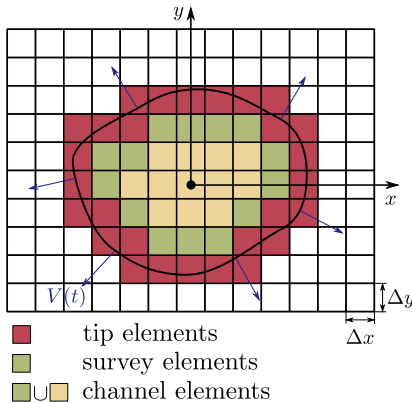


Figure 3 : Planar fracture on rectangular mesh.

Piece-wise constant approximation of fracture width:

$$w(x, y, t) = \sum_{m,n} w_{m,n}(t) H_{m,n}(x, y).$$

Lubrication equation:

$$\mathbf{w}(t) = \mathbf{w}(t - \Delta t) + \Delta t \mathbf{A}(\mathbf{w}) \mathbf{p} + \mathbf{S},$$

Splitting of variables:

$$\mathbf{w} = [\mathbf{w}^c, \mathbf{w}^t], \quad \mathbf{p} = [\mathbf{p}^c, \mathbf{p}^t], \quad \mathbf{S} = [\mathbf{S}^c, \mathbf{S}^t],$$

Elasticity equation:

$$\mathbf{p}^c = \boldsymbol{\sigma}_h^c + \mathbf{C}\mathbf{w},$$

Source / sink term:

$$\begin{aligned} S_{m,n}^c = & -2C'[\sqrt{t-t_{m,n}} - \sqrt{t-\Delta t-t_{m,n}}] + \\ & + \frac{\delta_{mm_0,nn_0}}{\Delta x \Delta y} Q(t) \Delta t. \end{aligned}$$

Locating the fracture front using the level set algorithm

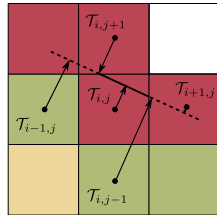


Figure 4 : Defining location of the moving piecewise linear fracture front.

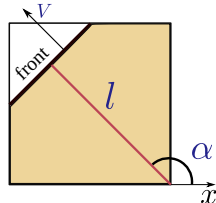


Figure 5 : Governing parameters of tip element.

Determining the distance to the front from centers of survey elements using the universal asymptotic solution:

$$\frac{s_i^2 V_i \mu'}{E'(w_i^s)^3} = g_\delta \left(\frac{K' s_i^{1/2}}{E' w_i^s}, \frac{2 s_i^{1/2} C'}{w_i^s V_i^{1/2}} \right), \quad V_i = \frac{s_i - s_{i,0}}{\Delta t}$$

Boundary conditions:

$$\mathcal{T}(x_i, y_i) = -s_i$$

Eikonal equation:

$$|\nabla \mathcal{T}| = \sqrt{\left(\frac{\partial \mathcal{T}}{\partial x}\right)^2 + \left(\frac{\partial \mathcal{T}}{\partial y}\right)^2} = 1$$

Upwind scheme for Eikonal equation:

$$\max \left(\frac{\mathcal{T}_{i,j} - \mathcal{T}_{i-1,j}}{\Delta x}, \frac{\mathcal{T}_{i,j} - \mathcal{T}_{i+1,j}}{\Delta x}, 0 \right)^2 +$$

$$\max \left(\frac{\mathcal{T}_{i,j} - \mathcal{T}_{i,j-1}}{\Delta y}, \frac{\mathcal{T}_{i,j} - \mathcal{T}_{i,j+1}}{\Delta y}, 0 \right)^2 = 1$$

Tip volume calculation

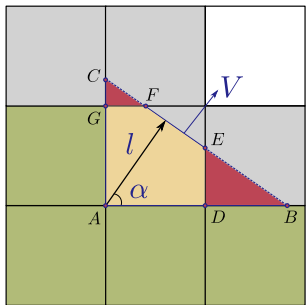


Figure 6 : Schematics of the procedure for tip volume calculation.

The average fracture width:

$$w^t = \frac{1}{\Delta x \Delta y} \begin{cases} \mathcal{V}_\Delta(\ell) - \mathcal{H}(\ell - \Delta y \sin \alpha) \mathcal{V}_\Delta(\ell - \Delta y \sin \alpha) \\ \quad - \mathcal{H}(\ell - \Delta x \cos \alpha) \mathcal{V}_\Delta(\ell - \Delta x \cos \alpha), & \alpha \neq 0, \pi/2, \\ \Delta y M_0(\ell), & \alpha = 0, \\ \Delta x M_0(\ell), & \alpha = \pi/2. \end{cases}$$

Comparison with reference radial solution

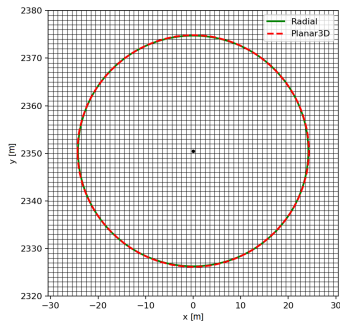


Figure 7 : Fracture footprints obtained by exact radial solution (solid green line) and Planar 3D ILSA (dashed red line).

$$E = 20 \text{ GPa}, \quad \nu = 0.25, \quad \mu = 0.01 \text{ Pa}\cdot\text{s}, \quad K_{IC} = 0.1 \text{ MPa}\cdot\text{m}^{1/2}, \\ C_l = 6.0 \cdot 10^{-5} \text{ m/s}^{-1/2}, \quad Q = 0.01 \text{ m}^3/\text{s}$$

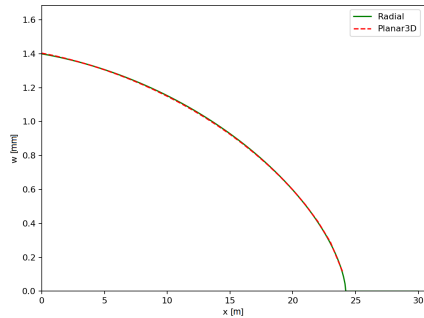


Figure 8 : Fracture opening obtained by exact radial solution (solid green line) and Planar 3D ILSA (dashed red line).

Comparison with experiment

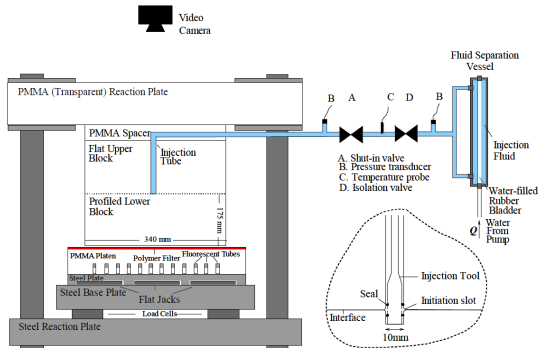


Figure 9 : Experiment scheme.

* R. Wu, A.P. Bunger, R.G. Jeffrey, E. Siebrits A comparison of numerical and experimental results of hydraulic fracture growth into a zone of lower confining stress // 42nd US Rock Mechanics Symposium and 2nd U.S.-Canada Rock Mechanics Symposium, San Francisco, June 29 — July 2, 2008, ARMA 08-267.

Comparison with experiment

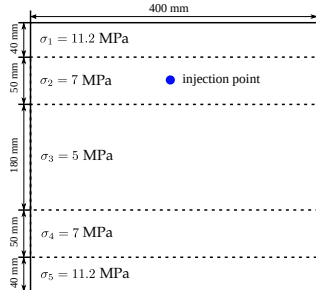


Figure 10 : Scheme of computational domain and distribution of confining stress in layers.

Figure 11 : Fracture width during simulation.

Comparison with experiment

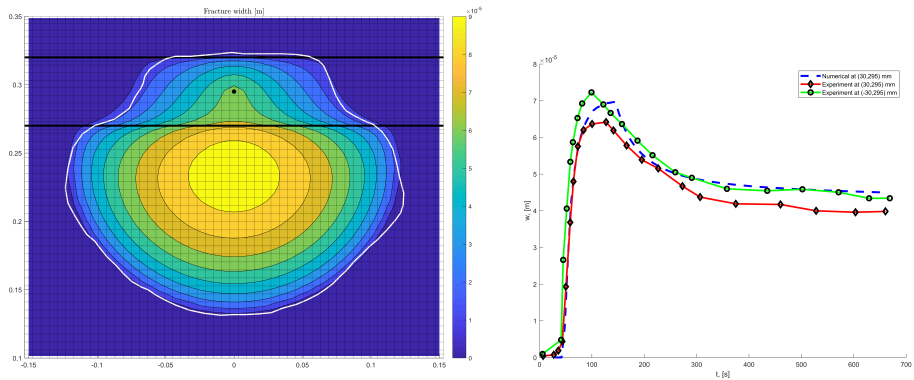


Figure 12 : Left: footprints comparison (white curve is the experimental data).
Right: comparison of the fracture width w at points $(-30, 295)$ mm and $(30, 295)$ mm.

High contrast of geological stresses

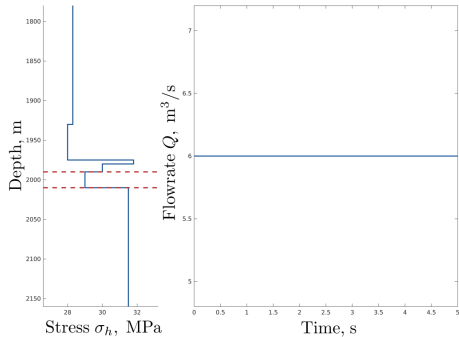


Figure 13 : Distribution of geological stresses σ_h over depth.

Symbol	Value	Unit
E	22	GPa
ν	0.23	1
K_{Ic}	1	$\text{MPa} \cdot \text{m}^{1/2}$
C_l	0	$\text{m} \cdot \text{s}^{-1/2}$

Table 1 : Common parameters for all layers.

Symbol	Value	Unit
K	0.05	$\text{Pa} \cdot \text{s}^n$
n	1	1

Table 2 : Parameters of the pumped fluid.

High contrast of geological stresses

Figure 14 : Fracture width.

Contact algorithm

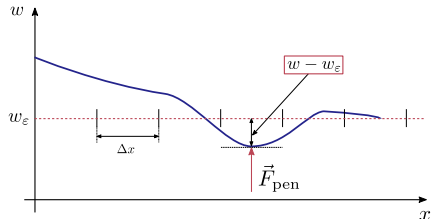


Figure 15 : Width at the begining of penalty iterations.

Contact force approximation:

$$F_{\text{pen}} = \frac{w - w_\varepsilon}{\delta} \chi[w < w_\varepsilon],$$

δ is penalty parameter, w_ε is width constraint, χ is indicator function.

Elasticity equation:

$$p(x, y, t) = \sigma_h(y) - \frac{E'}{8\pi} \int_{\mathcal{A}(t)} \frac{w(x', y', t) dx' dy'}{[(x' - x)^2 + (y' - y)^2]^{3/2}} + F_{\text{pen}}$$

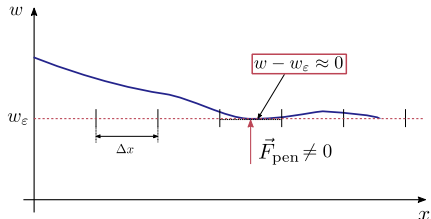


Figure 16 : Width at the end of penalty iterations.

Unconnected fractures due to leak-off

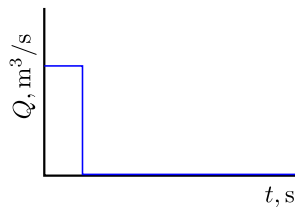
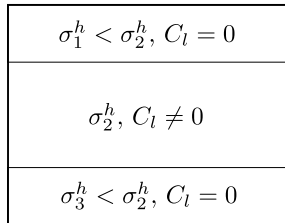


Figure 17 : Layers scheme and pumping schedule.

Figure 18 : Fracture width.

The coupled model of fracture growth and proppant transport, LIH

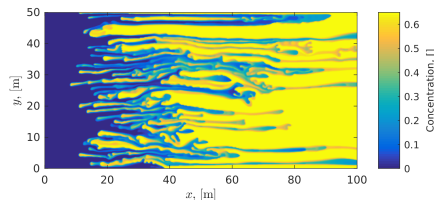
Fracture growth model

+

Fluid and proppant transport equations

$$\frac{\partial(c_f w)}{\partial t} + \frac{\partial}{\partial x}(c_f uw) + \frac{\partial}{\partial y}(c_f vw) = -q_\ell,$$

$$\frac{\partial(c_p w)}{\partial t} + \frac{\partial}{\partial x}(c_p uw) + \frac{\partial}{\partial y}(c_p vw) = 0,$$



More accurate solution of hydrodynamic \Rightarrow fine structures of «viscous fingering» (Saffman–Taylor instability), local bridging zones.

The details of proppant transport model refer to presentation of Pavel Kovtunenko and Arthur Skopintsev

The coupled model of fracture growth and proppant transport

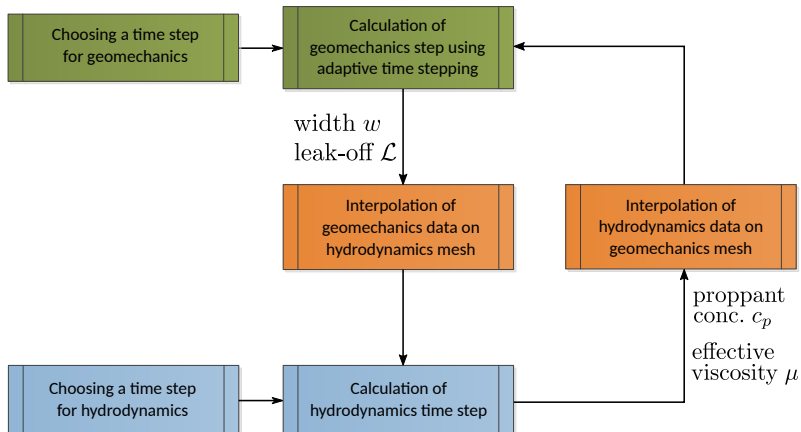


Figure 19 : Coupling scheme.

Pulsative injection

Figure 20 : Proppant concentration, pulses for 50 seconds of clean fluid and pulses for 100 seconds of fluid with proppant.

$$E = 22 \text{ GPa}, \quad \nu = 0.23, \quad \mu = 0.05 \text{ Pa}\cdot\text{s}, \quad K_{I_C} = 1 \text{ MPa}\cdot\text{m}^{1/2}, \\ C_l = 2.0 \cdot 10^{-5} \text{ m}\cdot\text{s}^{-1/2}, \quad Q = 0.06 \text{ m}^3/\text{s}$$

Figure 21 : Fracture width.

Fracture closure on the proppant

Figure 22 : Proppant concentration

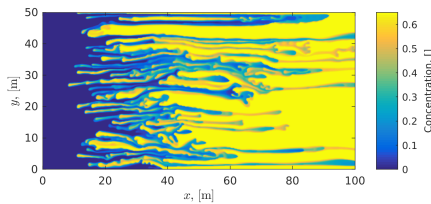
$$E = 30 \text{ GPa}, \quad \nu = 0.3, \quad \mu = 0.01 \text{ Pa}\cdot\text{s}, \quad K_{I_C} = 1 \text{ MPa}\cdot\text{m}^{1/2}, \\ C_l = 1.0 \cdot 10^{-4} \text{ m}\cdot\text{s}^{-1/2}, \quad Q_1 = 0.067 \text{ m}^3/\text{s}, \quad Q_2 = 0.0 \text{ m}^3/\text{s}$$

Figure 23 : Fracture width

Coupling with multi-component model of proppant transport, Skoltech

More advanced model accounts for:

- Multiple fluids
- Multiple proppants
- Proppant settling
- Gravitational convection
- Dynamic bridging



The details of proppant transport model refer to presentation of Sergey Boronin and other colleagues from Skoltech

Settling and gravitational convection case

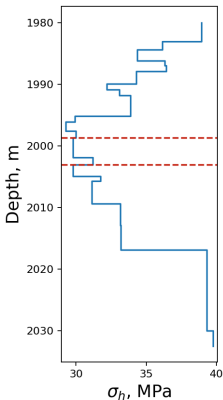


Figure 24 :
Distribution of geological
stresses σ_h over depth

Nº	t_{start}	t_{end}	K	n	Q
1	0	1380	0.1804	0.635	0.066
2	1380	1560	0.106	0.626	0.066

Table 3 : Parameters of the pumped fluid

Nº	t_{start}	t_{end}	d	ρ	$C_{p,\text{start}}$	$C_{p,\text{end}}$
1	180	300	0.689	2700	0.036	0.07
1	480	1380	0.689	2700	0.07	0.12

Table 4 : Parameters of the pumped proppants

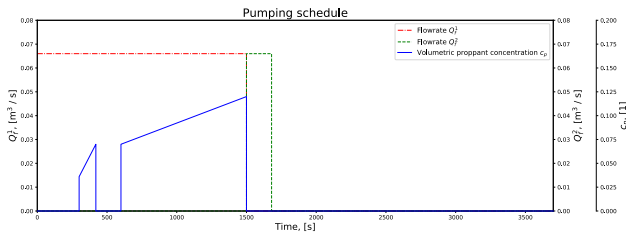


Figure 25 : Pumping schedule

Settling and gravitational convection case

Plans forward

- Taking into account heterogeneity of elasticity moduli
- Taking into account power-law fluid rheology
- Algorithm optimizations
- Calculation of multi-stage hydraulic fracturing
- Development of temperature model, taking into account degradation of the gel